Development of High Accuracy Millimeter Wave Components through Lithography Metal Manufacturing (LMM)

ESA-ESTEC Contract no 4000134183/21/NL/GLC/ov

ESA Technical Officer: Oilid Bouzekri, ESTEC, Noordwijk

Executive Summary

Document Data	
Project	Development of High Accuracy Millimeter Wave Components through Lithography Metal Manufacturing (DONE3D)
Document	Final Report
Issue 01	2023-07-17
Prepared by	Kay Reuter, Oscar Antonio Peverini, Mauro Lumia, Giuseppe Addamo,
Checked by	Oscar Antonio Peverini, Kay Reuter
Approved by	Kay Reuter
Electrically signed by	Kay Reuter Oscar Antonio Peverini

Document Change Record	
Issue 01	2023-07-17

CONTENTS

1 INTRODUCTION

1.1 Scope of the Document

This document contains the executive summary of the activity entitled "Development of High Accuracy Millimeter Wave Components through Lithography Metal Manufacturing (LMM) - DONE3D" carried out in the framework of the ESA-ESTEC Contract 4000134183/21/NL/GLC/ov.

1.2 Applicable Documents

AD1	ESA Contract No. 4000134183/21/NL/GLC/ov
AD2	Proposal "Idea I-2020-04519: 2nd Round: Development of high-accuracy millimeter-wave components through lithography metal manufacturing (LMM)"

1.3 Reference Documents

RD1	Y. Demers, et al. "Ka-Band User Antennas for VHTS GEO Applications", 2017 11th European Conference on Antennas and Propagation (EUCAP), 19-24 March 2017, Paris, France
RD2	B. Palacin et al. "Multibeam Antennas for Very High Throughput Satellites in Europe: Technologies and Trends", 2017 11th European Conference on Antennas and Propagation (EUCAP), 19-24 March 2017, Paris, France
RD3	P. Bosshard et al. "THALES ALENIA SPACE HTS/V-HTS Multiple Beam Antennas Sub-systems on the Right Track", 2016 10th European Conference on Antennas and Propagation (EuCAP), 10-15 April 2016, Davos, Switzerland
RD4	ESA ARTES Advanced Technology ref. 5B.193, "On-board Feed Chain for Combined Q, V-Band Feeder and Ka-band User Links"
RD5	R. Roberts et al. "Q/V-Band Feed System Development", 2016 10th European Conference on Antennas and Propagation (EuCAP), 10-15 April 2016, Davos, Switzerland
RD6	R. Roberts et al. "Multiple Spot Beam Reflector Antenna for High Throughput Satellites using Additive Manufacturing Technology", 2019 13th European Conference on Antennas and Propagation (EuCAP), 31 March-5 April 2019, Krakow, Poland
RD7	ESA ARTES Advanced Technology ref. 5B.182, "Radio-Frequency (RF) Feeds with Integrated RF, Mechanical and Thermal Functions"

1.4 Abbreviations and Acronyms

CNR	National Research Council of Italy
CTE	Coefficient of Thermal Expansion
CTS	Computer Tomography Scan
EDM	Electrical Discharge Machining
EO	Earth Observation
HTS	High Throughput satellites
LMM	Lithography Metal Manufacturing
LPBF	Laser Powder Bed Fusion
RF	Radio Frequency
SFB	Single Feed per Beam
VNA	Vector Network Analyzer

2 INTRODUCTION

2.1 Background

Current and next-generation EO missions are based on multi-feed, multi-frequency radiometric instruments operating from few GHz to hundreds of GHz, in order to achieve high resolution along with full on-ground coverage and high sensitivity. As an example, the MicroWave Imager (MWI) instrument of the MetOp-SG programme will consist of 18 channels operating from 18.7 GHz to 183 GHz, while the Copernicus Imaging Microwave Radiometer of the Copernicus Space Component Expansion programme will embark multi-beam, dual-band antenna-feed systems operating in C/X and K/Ka bands.

As far as SatCom are concerned, increasing data capacity is constantly required in order to be competitive with ground-based communications infrastructures [RD.1]. To this end, high (or very high) throughput satellites (HTS/VHTS) have replaced the traditional FSS/BSS platforms by exploiting higher frequency bands (Ka and Q/V). A typical service for telecommunication via geostationary satellite requires contiguous multiple-beam coverage over landmass (e.g. Europe, CONUS or a single country) exploiting a classical four colors schemes (2 orthogonal polarization, 2 sub-bands in Tx and Rx) [RD.2]. The required capacity can be achieved by exploiting larger antenna reflectors for reducing the coverage spot with a consequent high frequency re-use factor. The minimum spot-size is a trade-off between envelope/mass accommodation constraints in the satellite (which results in the maximum achievable reflector diameter and complexity of the focal plane) and the aggregate system capacity

Single-feed-per-beam (SFB) architectures are commonly used for the user links in K/Ka-band and for the feeder links in Q/V bands in order to achieve larger bandwidth and to reduce the number of gateway stations. For instance, as reported in [RD.3], an interesting scenario is based on 32 Ka-band user-beams in SFB configuration and 8 Q/V-band gateway-beams with 3 Ka-band reflectors of 3m5 class and one Q/V-band reflector of 2m4 class. Alternative solutions can be considered, where for example all the four reflectors are used for both the K/Ka-band user and Q/V-band feeder links. The latter antenna scheme requires the development of very complex and compact quadri-band antenna-feed systems operating simultaneously in K/Ka/Q/V bands that is the target of the ARTES activity [RD.5].

In this framework, the applicability of the LMM technology to the manufacturing of feed-system components and subassemblies is particularly interesting in view of developing monolithic architectures that are more beneficial w.r.t. spit-block architectures [RD.5] in terms of mass, envelope, lead time and cost, AIT procedures, and power-handling. An example of these benefits in Ku band is reported in [RD.6], where a cluster of 18 feeds for a three-reflectors SFB antenna has been manufactured through SLM with a mass reduction greater than 80% w.r.t. conventional manufacturing methods. Antenna-feed system integration is also the target of the ARTES activity [RD.7], where integration of RF, thermal and structural functionalities is required.

2.2 Objectives

The present project has been promoted by the Open Channel Early Technology Programme of the European Space Agency (ESA), with the main goal of investigating a new AM supply chain that is based on the LMM technology in conjunction with copper. This material was not available for the LMM process prior to this activity.

The study, kicked-off on May 2021, is executed by a team composed of two partners: the IFAM institute of Fraunhofer (Germany), acting as the Prime, and the IEIIT institute of CNR (Italy).

The main expected advantages of the LMM process with respect to currently available AM technologies, which have been investigated in this activity, are good surface finishing, suitable dimensional tolerances, and good mechanical properties. To this end, the RF characteristics of the printed parts shall be derived in K and Ka band (18 – 30 GHz), along with other material and mechanical parameters of interest, among which are porosity, mechanical strength, and manufacturing errors. Based on the measured performances of the functional samples, the LMM manufacturing route shall be tuned with the goal of improving mainly dimensional accuracy and electrical conductivity.

In Phase B of the activity, a RF demonstrator shall be designed and tested in laboratory conditions. It consists of a low-pass filter in WR28 waveguide operating in Ka band.

2.3 Methodology

The present study has been carried out according to the workflow reported in Figure 1, which consists of two phases:

- Phase A - Proof of Concept.
- Phase B - Demonstration of Feasibility and Use.

In Phase A, the first goal has been the implementation of the complete route (from material preparation to sintering) of the copper-based Lithography Metal Manufacturing (LMM) process. This has been carried in WP A1.

To assess the material and mechanical properties of the process, non-functional samples (bricks, rods) have been first manufactured and tested. Next, simple vehicles for testing the properties relevant for the intended RF application have been designed, manufactured and tested in WPA2 and WPA3. To optimize the LMM process for RF applications, three manufacturing jobs has been iteratively carried out on the basis of the outcomes of the RF testing campaigns.

As an output of the Phase A activities, the main parameters of interest of LMM parts have been derived, including are electrical conductivity, surface roughness, dimensional accuracy, minimum feature size, and repeatability. Based on these outcomes, in Phase B a demonstrator (namely a WR28 waveguide filter) has been selected and designed to assess the feasibility and use of the LMM technology in the development of RF space components. The measured performance of two demonstrator prototypes have been compared against the simulations of the nominal model and of the geometries de-embedded through computer tomography scan. Finally, way-forward activities have been identified to further improve the LMM process and its applicability to RF space applications.

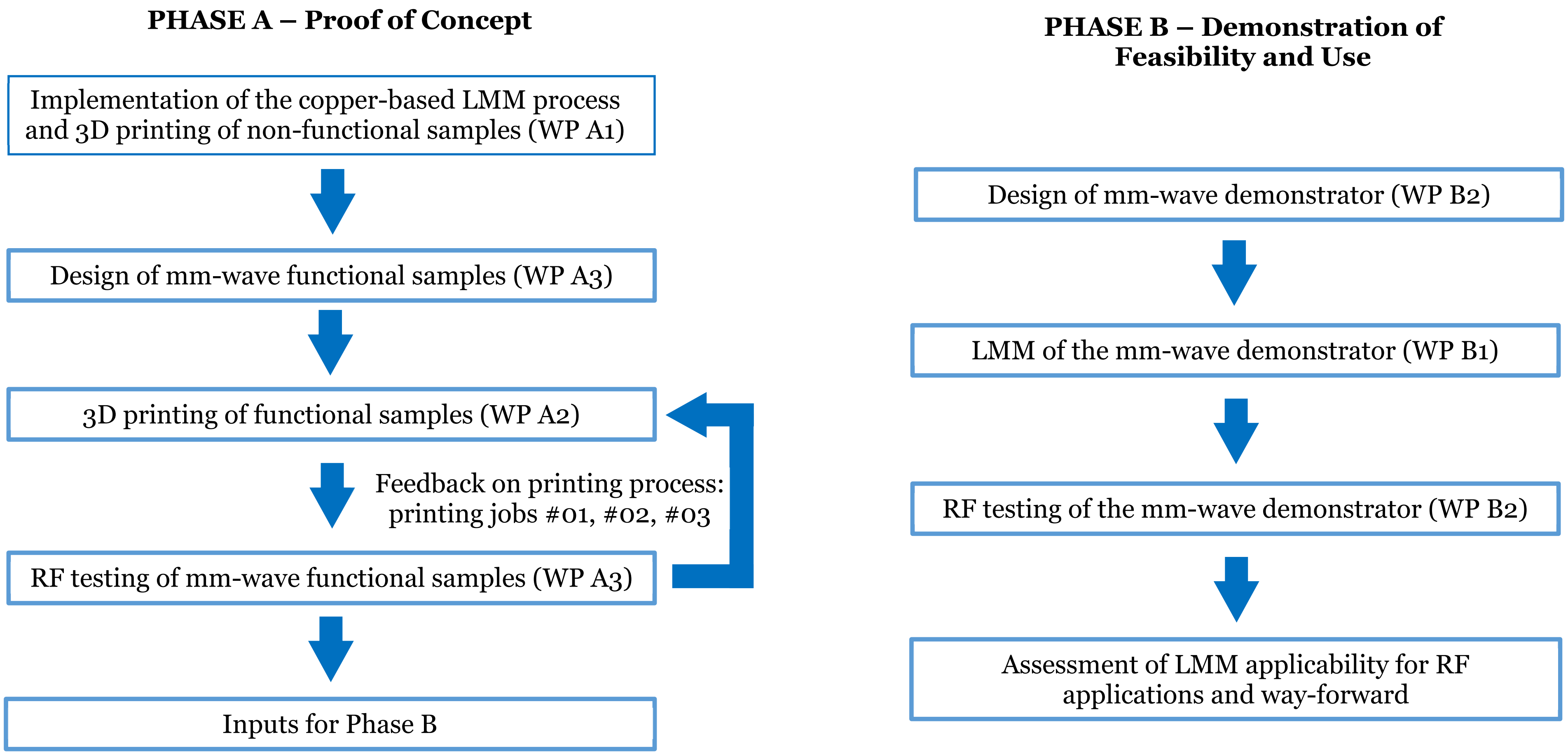

Figure 1: Workflow of the study activity.

3 MAIN ACHIEVEMENTS

3.1 Implementation of the End-to-End Copper-based LMM Process

In the Done3D project, the suitability of the LMM (lithography-based metal manufacturing) process for the production of high frequency filters was investigated. For this purpose, a process route for copper was developed. This included the selection of a suitable copper powder, the optimization of the powder loading of the photosensitive feedstock and the subsequent printing process. The debinding process was optimized using FTIR measurements in order to remove the organic components of the printed components as residue-free as possible. Sintering of the components was carried out in reducing atmosphere under hydrogen at a temperature of 1050°C.

The developed process route can produce components with the following properties:

- density of the sintered parts. 98,7%

- line roughness: 2-4 µm

- minimal wall thickness: > 150µm

- electrical conductivity: 86% IACS

3.2 Development of Test Cavities

To assess the RF properties of the copper-based LMM process, the following functional samples have been designed, manufactured, and tested:

- WR42 waveguide cavity resonator operating at 20 GHz.
- WR28 waveguide cavity resonator operating at 30 GHz.

Each test cavity exhibits a reflection zero and two transmission zeros. The latter are generated almost independently by the two stub resonators that are arranged along the opposite sides of the rectangular waveguide. This arrangement reduces the multi-modal interaction between the stub resonators, thus leading to a simpler de-embedding procedure of the manufactured geometry on the basis of the measured performances.

Several single-cavity resonators have been developed in different manufacturing jobs with the aim of optimizing the LMM process. Figure 2 shows some of the WR28-waveguide samples, whereas Figure 3 reports the comparison between the measured and simulated scattering parameters of one of the de-embedded geometries.

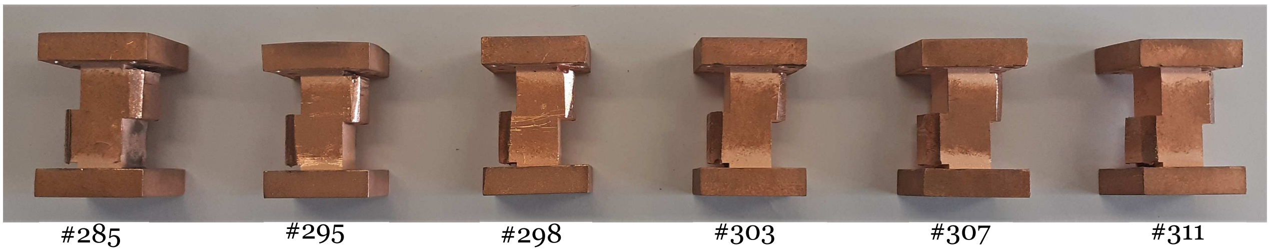

Figure 2: WR28 waveguide resonator prototypes

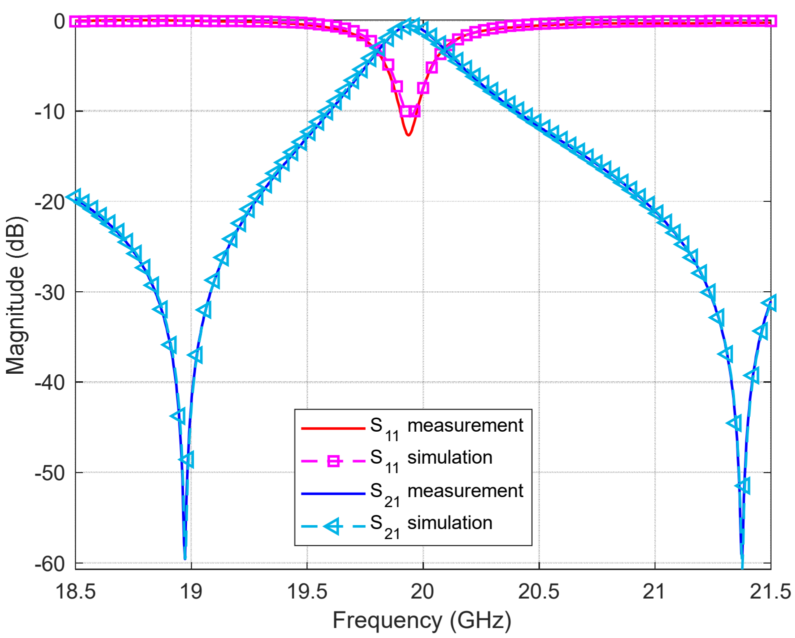

Figure 3: Comparison between measured and simulated scattering parameters for the de-embedded geometry of the prototype #348.

The summary of the dimensional errors and de-embedded equivalent surface electrical resistivity ρ of the printed test cavities in WR28 and WR42 is reported in Table 1.

Waveguide	**Part ID**	**Job ID**	**ΔwgA_A** (mm)	**ΔwgB_A** (mm)	**ΔwgA_B** (mm)	**ΔwgB_B** (mm)	**ΔwgS1** (mm)	**ΔwgS2** (mm)	**ΔLwk** (mm)	**Mean error value** (mm)	**ρ** (μΩ cm)
WR28	#285	1	-0.392	+0.024	-0.492	-0.186	+0.081	-0.071	+0.055	0.186	22
WR28	#295	2	-0.812	-0.156	-0.562	-0.006	-0.022	-0.134	-0.153	0.264	9
WR28	#298	2	-0.312	+0.044	-0.412	-0.006	-0.106	-0.359	-0.03	0.181	11
WR28	#303	2	-0.512	+0.044	-0.462	-0.056	-0.065	-0.203	-0.105	0.207	11
WR28	#307	2	-0.512	-0.056	-0.412	-0.056	-0.063	-0.22	-0.25	0.224	6
WR28	#311	2	-0.562	-0.156	-0.512	-0.056	-0.065	-0.202	-0.245	0.257	8
WR28	#347	3	0.288	0.344	0.088	0.244	0.188	-0.142	0.065	0.194	10
WR42	#348	3	0.032	0.082	0.132	0.382	0.307	-0.415	0.2	0.221	10

Table 1: Summary of the dimensional errors of the printed prototypes and de-embedded equivalent surface electrical resistivity ρ.

3.3 Development of WR28 Waveguide Filters

To assess the applicability of the LMM process to RF space applications, the two prototypes of WR28 waveguide filter shown in Figure 4 have been designed, manufactured and tested. Figure 5 Comparison between the measured and nominal scattering parameters for the WR28 filter prototype #470.

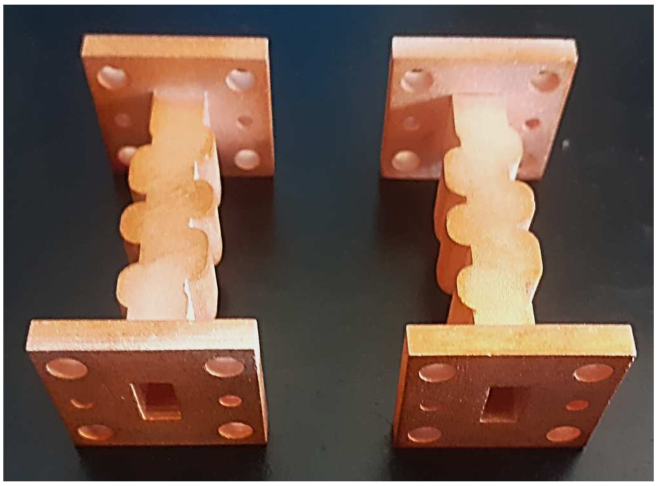

#470 #471

Figure 4: WR28 filter prototypes.

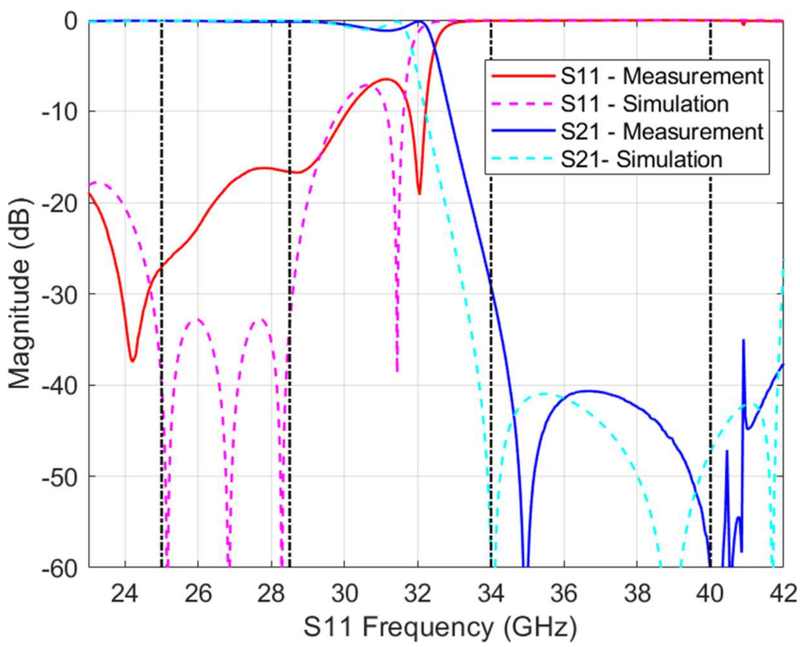

Figure 5: Comparison between the measured and nominal scattering parameters for the WR28 filter prototype #470.

To better understand the deviation of the measured responses exhibited by the two WR28 filters from the predicted performance, both prototypes have been subjected to Computed

Tomography Scan (CTS). Figure 6 shows the de-embedded CAD model used in the RF simulations and the comparison between the measured and simulated scattering parameters for the de-embedded geometry of filter #470

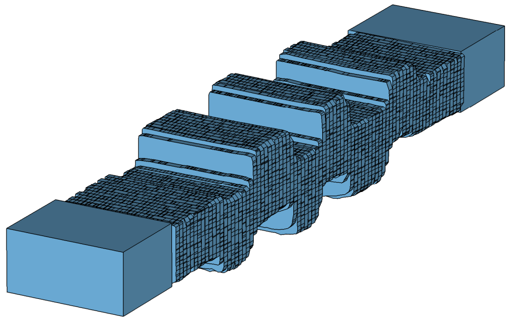

(a)

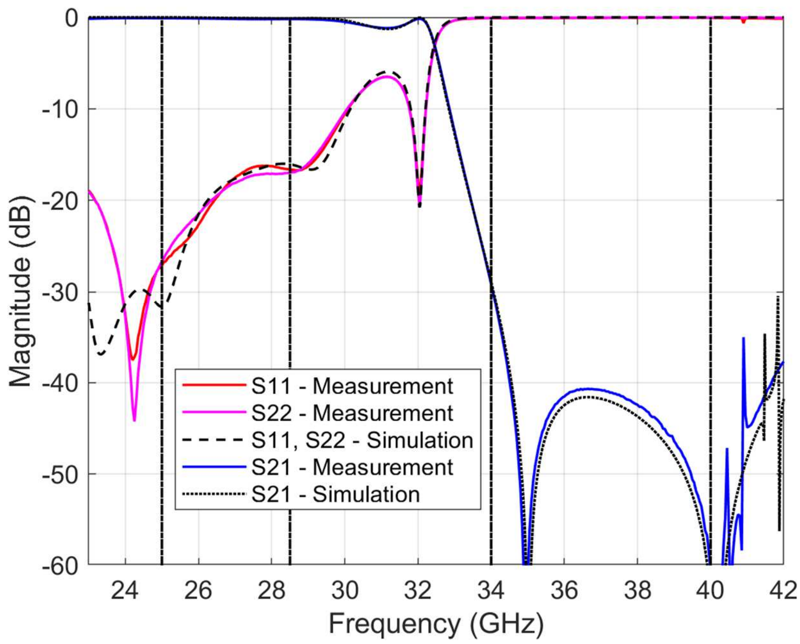

(b)

Figure 6: CTS analysis of the filter prototype #470. (a) De-embedded CAD model used in the RF simulations. (b) Comparison between the measured and simulated scattering parameters for the de-embedded geometry.

4 CONCLUSION

Table 2 reports a comparison among standard machining and 3D-printing technologies that today are mostly used or investigated to manufacture RF space and the copper-based LMM process developed in the present study. The table includes the main mechanical, thermal and electrical parameters of interest for RF space applications.

Standard machining includes milling, turning and Electrical Discharge Machining (EDM). All these processes can provide RF parts directly in aluminium alloys (e.g., 6000 series) with high accuracy, good surface finishing, high mechanical and thermal properties, along with a TRL equal to 9. These technologies require split/block or multi/layer layouts that result in massive components.

A possible solution to achieve monolithic components with complex inner shapes is electroforming. This technology provides accurate and near-net-shape components built in copper and gold-passivated. The main drawbacks are the high mass and lead time/costs.

To overcome the limitations exhibited by electro-forming, the LPBF process can be applied, since it allows for the development of all-metal monolithic components in aluminium with almost the same mechanical and thermal properties as those provided by standard machining.

With respect to the LPBF process, the copper-based LMM developed in this activity has the main advantage of providing better surface finishing (in the order of 1 - 3 μm), although the dimensional accuracy is worse (up to 0.18 mm).

This study has increased the TRL of LMM printing of RF components from 2 to 3. Improvements in the sintering process and development of more complex radio-frequency structures can be targeted in next activities aimed at higher TRLs. Specifically, the current implementation of the LMM process relies on copper, which suffers from high weight and interfacing issues with other metal parts that may generate passive intermodulation products. Consequently, next activities shall include the development of an aluminium-based LMM route, which is a highly challenging activity because of some technological aspects (e.g., the de-binding process).

Process	**Milling/turning**	**Electric discharge machining**	**Electroforming**	**LPBF**	**LMM**
Material	6000 series aluminum alloy	6000 series aluminum alloy	copper	AlSi7Mg, AlSi10Mg, Scalmalloy	copper
Dimensional accuracy	5 - 20 µm	5 - 20 µm	1 - 5 µm	40 - 80 µm	50 - 180 µm
Surface roughness R_a	0.4 - 0.8 µm	0.8 - 1.6 µm	0.4 - 1.0 µm	3 - 8 µm	1 - 3 µm
Surface electrical resistivity (10 - 30 GHz)	4 - 6 µΩ cm	6 - 8 µΩ cm	3 - 5 µΩ cm (with gold passivating layer)	10 - 16 µΩ cm (without plating)	10 - 18 µΩ cm
Melting point metal	650 °C	650 °C	1083 °C	570 - 580 °C	1083 °C **(TBC)**
Coefficient of linear thermal expansion	$22 - 24 \cdot 10^{-6}$ K^{-1}	$22 - 24 \cdot 10^{-6}$ K^{-1}	$16 - 19 \cdot 10^{-6}$ K^{-1}	$20 - 24 \cdot 10^{-6}$ K^{-1}	$16 - 19 \cdot 10^{-6}$ K^{-1} **(TBC)**
Thermal conductivity	170 - 200 W/m/K	170 - 200 W/m/K	385 - 400 W/m/K	180 - 190 W/m/K	385 - 400 W/m/K **(TBC)**
Density	2.7 g/cm³	2.7 g/cm³	8.9 g/cm³	2.7 g/cm³	8.9 g/cm³ **(TBC)**
Tensile strength	260 - 310 MPa	260 - 310 MPa	200 - 360 MPa	230 - 450 MPa	200 - 360 Mpa **(TBC)**
Near-net shapes (envelope, mass)	massive	massive	near-net shapes	near-net shapes	near-net shapes
Mechanical layout	split-block, multi-layer	split-block, multi-layer	monolithic	monolithic	monolithic
Lead time/cost	medium	medium	high	low	Low
TRL	9	9	9	8-9	3

Table 2: Comparison among standard machining and AM technologies mostly exploited for the manufacturing of RF space components and the copper-based LMM process developed in the present activity.

END OF DOCUMENT